Journal of Materials Chemistry B

Accepted Manuscript

ROYAL SOCIETY OF CHEMISTRY

www.rsc.org/materialsB

Journal Name

RSCPublishing

ARTICLE

Near-infrared Fluorescent Probes Based on Piperazine-Functionalized BODIPY Dyes for Sensitive Detection of Lysosomal pH

Cite this: DOI: 10.1039/xoxxoooooox

Received ooth January 2015,
Accepted ooth January 2015

DOI: 10.1039/xoxxoooooox

www.rsc.org/

Jingtuo Zhang[a], Mu Yang[a], Cong Li[a], Nethaniah Dorh[a], Fei Xie[a], Fen-Tair Luo*[b], Ashutosh Tiwari*[a], and Haiying Liu*[a]

Three acidotropic, near-infrared fluorescent probes based on piperazine-modified BODIPY dyes (**A**, **B** and **C**) have been developed for sensitive and selective detection of lysosomal pH in living cells. Probes **A** and **B** display low solubilities in aqueous solutions while probe **C** is highly water-soluble. The fluorescent responsive mechanism of these probes to lysosomal pH is based on intramolecular charge transfer (ICT) and potential photoinduced electron transfer from piperazine moieties at 3,5-positions to BODIPY cores in near-infrared region. The sensitivity and selectivity of the probes to pH over metal ions have been investigated by spectroscopic analysis in aqueous solutions. The probes have low auto-fluorescence at physiological pH condition while their fluorescence intensities significantly increase when pH is shifted to acidic condition. Furthermore, these three probes were successfully applied to the *in vitro* lysosome imaging inside normal endothelial and breast cancer cells.

1. Introduction

Lysosomes, membrane-delimited, acidic organelles present in essentially all eukaryotic cells, employ more than 70 hydrolytic enzymes to degrade biological macromolecules taken up by endocytosis, phagocytosis and autophagy.[1-3] Significant disruption in the lysosomal pH can cause lysosome malfunction and thus cause lysosomal storage diseases.[4] Therefore, it is very important to precisely detect lysosomal pH in living cells in order to study cellular functions for insightful understanding of physiological and pathological processes. Fluorescence spectroscopy employing pH-sensitive fluorescent probes is becoming one of the most powerful tools for monitoring intracellular pH, and possesses many technical and practical advantages over other methods because it can detect the intracellular pH of intact cells and subcellular regions with operational simplicity, high sensitivity, and excellent spatial and temporal resolution.[5-15] Only a few of them have been applied to detect lysosomal pH inside living cells even though many fluorescent probes for pH have been prepared.[16-21] Most fluorescent probes are selectively accumulated in acidic lysosomes via lysosomotropism where their tertiary amine residues are protonated in a cellular acidic environment.[12] The protonation of ionizable tertiary amine groups on the fluorophores in acidic lysosomes enhances the probe fluorescence through the suppression of photo-induced electron transfer from the tertiary amine to the probe fluorophores.[9, 22-26] The potential drawback for these fluorescent probes is their broad pH responses and relative high fluorescent background at pH 7.4. Recent approach to address this high fluorescent background at pH 7.4 is to use fluorescein and Rhodamine dyes by taking advantages of low fluorescence background at pH 7.4 because of the ‘‘ring-closed’’ state of spirolactam rings in the fluorophores at pH 7.4.[6, 7, 14, 27] However, most fluorescent probes are not soluble in aqueous solution, and some of them can cause cell damage due to their short absorption and emission wavelengths with less than 600 nm as very few near-infrared fluorescent probes for lysosomal pH in living cells were reported.[28-30] In order to address these issues of high fluorescent background and potential cell damage, we reported Rhodamine dye counterparts with near-infrared excitation and emission wavelengths as fluorescent probes for lysosomal pH in living cells.[31] We have demonstrated the feasibility of near-infrared fluorescent probes with spirocyclic structures for sensitive detection of lysosomal pH in living cells with advantages of excellent photostability, low cytotoxicity, deep tissue light penetration and low autofluorescence background.[31] Under neutral or basic conditions, the fluorescent probes retain the spirocyclic form that is non-fluorescent and colorless. Acidic environment effectively leads to ring opening of the spirocyclic form in fluorescent probes, and results in strong fluorescence. However, these fluorescent probes are still insoluble in aqueous solution.[31]

The search for readily accessible near-infrared fluorescent probes with good water solubility, large dynamic range and high specificity is still a challenging task for near-infrared imaging of lysosomal pH in living cells. In this paper, we design and prepare near-infrared fluorescent probes for lysosomal pH by using piperazine residues to manipulate the fluorescent responses of the probes to pH via modulation of intramolecular charge transfer (ICT) effect and potential photoinduced electron transfer of piperazine moieties at 3,5-positions to BODIPY cores at different pH values. Piperazine residues were incorporated into BODIPY dyes at 3,5-positions as parts of BODIPY cores while tri(ethylene glycol)methyl ether residues attached to piperazine moieties were used to enhance hydrophilic properties of the probes and improve water solubility of the probes. Fluorescent probes display very weak fluorescence because of strong intramolecular charge transfer from piperazine residues to BODIPY cores at neutral pH, and potential photo-induced electron transfer from lower part nitrogen atoms of piperazine groups to BODIPY core. Decrease of pH significantly enhances fluorescence intensity because the pronation of piperazine residues at acidic pH considerably reduces intramolecular charge transfer effect of the piperazine residues to BODPY cores, and the potential photo-induced electron transfer effect. These fluorescent probes have advantages such as high photostability, sensitive and selective near-infrared imaging of lysosomal pH in living cells with potential intact *in vivo* imaging and deep tissue penetration without auto-fluorescence and unintended cellular damage issues.

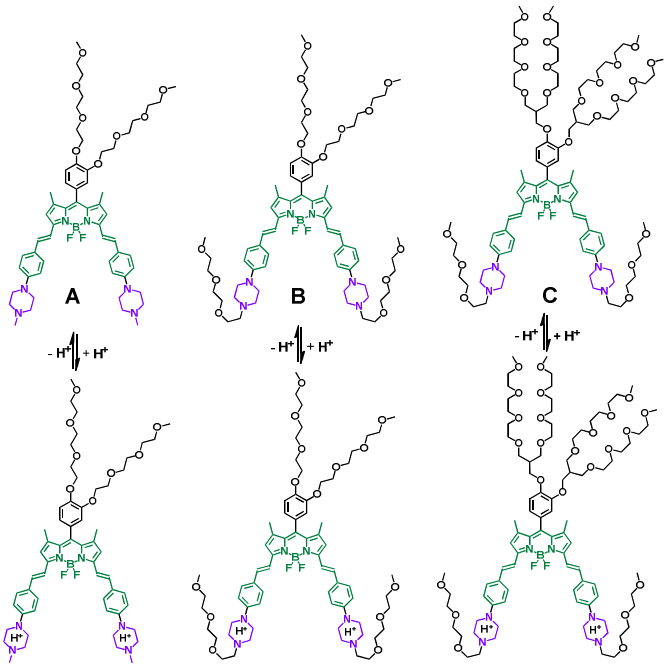

Scheme 1 Chemical structures of near-infrared fluorescent probes and their responses to pH.

2. Experimental Section

2.1 Instrumentations:

^{1}H NMR and ^{13}C NMR spectra were collected on 400 MHz Varian Unity Inova NMR spectrophotometer instrument. ^{1}H and ^{13}C NMR spectra were recorded in $CDCl_3$ and DMSO-d_6. Chemical shifts (δ) were given in ppm relative to solvent residual peaks (^{1}H: δ 7.26 for $CDCl_3$, δ 2.50 for DMSO-d_6; ^{13}C: δ 77.3 for $CDCl_3$) as internal standard. HRMS were measured with electrospray ionization (ESI) mass spectrometer and electron impact ionization (EI) mass spectrometer. Absorption spectra were taken on a Perkin Elmer Lambda 35 UV/VIS spectrometer. Fluorescence spectra were recorded on a Jobin Yvon Fluoromax-4 spectrofluorometer. The potential aggregation behaviors of probes **A**, **B** and **C** in aqueous solutions were determined by dynamic light scattering (Coulter NP4 Plus, Beckman Coulter, Fullerton, CA).

2.2 Materials:

Unless specifically indicated, all reagents and solvents were obtained from commercial suppliers and used without further purification. BODIPY dyes **7** and **9** were prepared from compounds **6** and **8** respectively, according to our previous reported procedures[32, 33]

General procedure to prepare fluorescent probe A, B and C: When BODIPY dye **7** or **8** (1 eq.), compound **3** or **5** (6 eq.) were dissolved in benzene, a small amount of piperidine and acetic acid were added into the solution and the reaction mixture was refluxed for 10-16 hours at 100 °C. Any water formed during the reaction was removed azeotropically by using a Dean-Stark apparatus. After the reaction was quenched by water at room temperature, the mixture was concentrated under reduced pressure and re-dissolved in 100 mL dichloromethane. It was sequentially washed with water (2 x 100 mL) and brine (100 mL), dried over Na_2SO_4 and filtered. The filtrate was concentrated under reduced pressure and the crude product was purified by column chromatography with silica gel (32-63 microns, 230-400 mesh) by using CH_2Cl_2/MeOH (7/1, v/v) as eluent to obtain fluorescent probes **A**, **B** or **C**:

Fluorescent probe A: According to the general procedure, fluorescent probe **A** was prepared from BODIPY dye **7** (50 mg, 0.077 mmol), compound **3** (95 mg, 0.465 mmol), benzene (8 mL), piperidine (0.1 mL, 1.012 mmol) and acetic acid (0.1 mL, 1.747 mmol). The mixture was refluxed for 10 hours. After work-up and purification by column chromatography by using CH_2Cl_2/MeOH/Et_3N (7/1/0.01, v/v/v) as eluent, probe **A** was obtained as green solid (33 mg, 42%). ^{1}H NMR (400 MHz, $CDCl_3$) δ 7.67 – 7.49 (m, 6H), 7.25 – 7.12 (m, 2H), 6.99 (d, J = 8 Hz, 1H), 6.95 – 6.87 (m, 5H), 6.84 (d, J = 8 Hz, 1H), 6.60 (br s, 2H), 4.22 (t, J = 4.8 Hz, 2H), 4.15 (t, J = 4.8 Hz, 2H), 3.92 (t, J = 4.8 Hz, 2H), 3.86 (t, J = 4.8 Hz, 2H), 3.81 – 3.49 (m, 16H), 3.42 – 3.30 (m, 14H), 2.68 (br s, 8H), 2.43 (s, 6H), 1.51 (s, 6H); ^{13}C NMR (100 MHz, $CDCl_3$) δ 152.9, 151.4, 149.8, 149.7, 141.7, 136.1, 133.6, 129.2, 128.4, 128.3, 122.0,

117.6, 116.8, 115.7, 115.2, 114.7, 72.2, 72.2, 71.2, 71.0, 70.9, 70.1, 70.0, 69.4, 69.0, 59.3, 54.9, 48.1, 46.0, 15.0. HRMS (ESI): calculated for $C_{57}H_{75}BF_2N_6O_8$ $[M]^+$, 1020.5702; found, 1020.5736.

Fluorescent probe B: According to the general procedure, fluorescent probe **B** was prepared from BODIPY dye **7** (50 mg, 0.077 mmol), compound **5** (157 mg, 0.467 mmol), benzene (10 mL), piperidine (0.1 mL, 1.012 mmol) and acetic acid (0.1 mL, 1.747 mmol). The mixture was refluxed for 10 hours. After work-up and purification by column chromatography by using CH_2Cl_2/MeOH (7/1, v/v) as eluent, probe **B** was obtained as green oil (51 mg, 52%). ^{1}H NMR (400 MHz, $CDCl_3$) δ 7.60 – 7.47 (m, 6H), 7.16 (d, J = 16 Hz, 2H), 6.97 (d, J = 8 Hz, 1H), 6.91 – 6.85 (m, 5H), 6.81 (d, J = 8 Hz, 1H), 6.59 (s, 2H), 4.20 (t, J = 4.8 Hz, 2H), 4.12 (t, J = 4.8 Hz, 2H), 3.89 (t, J = 4.8 Hz, 2H), 3.84 (t, J = 4.8 Hz, 2H), 3.79 – 3.47 (m, 36H), 3.38 – 3.36 (m, 9H), 3.32 (s, 3H), 3.30 (br s, 8H), 2.75 – 2.64 (m, 12H), 1.49 (s, 6H); ^{13}C NMR (100 MHz, $CDCl_3$) δ 152.8, 151.6, 149.7, 149.6, 142.8, 141.5, 137.1, 136.1, 133.5, 130.1, 129.0, 128.4, 127.9, 125.6, 121.9, 117.5, 116.5, 115.4, 115.2, 115.0, 114.6, 72.2, 72.1, 71.1, 70.9, 70.8, 70.7, 70.6, 70.0, 69.9, 69.3, 69.1, 68.9, 59.3, 59.2, 48.3, 47.9, 14.9. HRMS (ESI): calculated for $C_{69}H_{99}BF_2N_6O_{14}$ $[M]^+$, 1284.7274; found, 1284.7261.

Fluorescent probe C: According to the general procedure, fluorescent probe **C** was prepared from BODIPY dye **9** (50 mg, 0.045 mmol), compound **5** (90 mg, 0.268 mmol), benzene (8 mL), piperidine (0.1 mL, 1.012 mmol) and acetic acid (0.1 mL, 1.747 mmol). The mixture was refluxed for 16 hours. After work-up and purification by column chromatography by using CH_2Cl_2/MeOH (7/1, v/v) as eluent, probe **C** was obtained as green oil (30 mg, 38%); ^{1}H NMR (400 MHz, DMSO-d_6) δ 7.50 – 7.41 (m, 6H), 7.35 (d, J = 16 Hz, 2H), 7.13 (d, J = 8 Hz, 1H), 7.04 – 6.97 (m, 5H), 6.91 – 6.87 (m, 3H), 4.06 (d, J = 8 Hz, 2H), 4.01 (d, J = 8 Hz, 2H), 3.62 – 3.36 (m, 76H), 3.34 – 3.18 (m, 26H), 2.59 (br s, 12H), 2.31 (sextet, J = 5.6 Hz, 1H), 2.25 (sextet, J = 5.6 Hz, 1H) 1.50 (s, 6H); ^{13}C NMR (100 MHz, $CDCl_3$) δ 152.9, 151.5, 149.9, 149.8, 142.7, 141.7, 137.6, 136.0, 133.6, 130.1, 129.1, 128.3, 127.9, 121.5, 117.5, 116.7, 115.6, 114.3, 113.9, 72.2, 72.2, 71.1, 70.9, 70.9, 70.8, 70.7, 70.7, 69.7, 69.6, 67.8, 67.4, 59.3, 59.2, 57.9, 48.1, 32.2, 23.0, 15.1, 14.4. HRMS (ESI): calculated for $C_{91}H_{143}BF_2N_6O_{24}$ $[M]^+$, 1753.0209; found, 1753.0194.

2.3 Optical measurements

All absorption and emission spectra were recorded by using standard 1 cm path length quartz fluorescence cuvette at room temperature. The slit widths of excitation and emission were set to 3 nm and 5 nm respectively, and the excitation wavelength is set at 620 nm for fluorescence spectroscopies. 1.0 mM DMSO solutions of fluorescent probes **A** and **B** and 1.0 mM aqueous solution of probe **C** were used as stock solutions. All optical spectra of fluorescent probes **A**, **B** and **C** were measured in the 50 mM citrate-phosphate buffer solutions (contain 0.5% DMSO from stocks for fluorescent probes **A** and **B**).

2.4 Cell culture and fluorescence imaging

Breast cancer cells MDA-MB-231 and normal endothelial cells HUVEC-C (from ATCC) were cultured as previously described.[34] In brief, cells were plated on 12-well culture plates at 1 x 10^5 cells/well and incubated at 37 ^{o}C in 5% CO_2 incubator overnight. Next day, the media was removed and cells were rinsed twice with 1 X PBS after which fresh serum-free media was added and cells were incubated for 2 h at 37 ^{0}C in CO_2 incubator. Following 2 h serum starvation, fresh serum free media with/without 2 μM, 5 μM, 10 μM probe **A** or 5 μM, 15 μM, 25 μM probe **B** or **C** were added and incubated further with cells for 2 h. Live cell images were acquired using an inverted fluorescence microscope (AMF-4306, $EVOS_{fl}$, AMG) with DAPI filter for Hoechst 33342 (Sigma-Aldich), GFP filter for LysoSensor Green DND-189 (Invitrogen), and CY5 filter for fluorescent probes **A**, **B**, and **C**. The fluorescence images were obtained at 40x and 60x magnification for HUVEC-C and at 60x magnification for MDA-MB-231 cells. The exposure times for each filter were kept constant. Co-localization analysis based on Pearson's coefficient was done using JACoP plugin from ImageJ.[35]

Live cell fluorescence imaging at different intracellular pH: Normal endothelial cells HUVEC-C (from ATCC) were cultured as previously described. In brief, cells were plated on 12-well culture plates at 1 x 10^5 cells/well and incubated at 37 ^{o}C in 5% CO_2 incubator overnight. Next day, when the media was removed and cells were rinsed twice with 1 X PBS (pH 7.4), fresh serum free media with 5 μM probe **A** or 15 μM probe **B** or 15 μM probe **C** was added and incubated further with cells for 2 h. After incubation, the medium was removed and cells were gently rinsed with PBS (pH 7.4) three times. It was then treated with nigericin (5 μg/mL) in 2 mL potassium rich PBS at different pH values of 5.0, 5.5, 6.5, and 7.5, and incubated further for 15 min. Live cell images were acquired using an inverted fluorescence microscope (AMF-4306, EVOSfl, AMG) with DAPI filter for Hoechst 33342 (Sigma-Aldich), GFP filter for LysoSensor Green DND-189 (Invitrogen), and CY5 filter for fluorescent probes **A**, **B**, and **C**. The fluorescence images were obtained at 40x magnification. The exposure times for each filter were kept constant.

2.5 Determination of cellular uptake efficiency

HUVEC-C cells were plated at a density of 1 × 10^4 cells/well on a 96-well cell culture plate and incubated at 37 ^{o}C in 5% CO_2 incubator overnight. Next day, the culture medium was removed and cells were rinsed twice with PBS (pH 7.4). Fresh 100 μL media with 2 μM, 5 μM, 10 μM of probe **A**, or 5 μM, 15 μM, 25 μM of probe **B** or 5 μM, 15 μM, 25 μM of probe **C** were added to the wells in triplicate and incubated for 2 h. Controls and blanks were also set in triplicate at the same time. Controls had culture media and dyes but no cells. Blanks used for background subtraction had cells and media but no dyes. After 2 h incubation the media (100 μL) was pipetted out from the plate and put in a fresh 96-well plate. Each well was rinsed with 100 μL of fresh PBS (pH 7.4) and the solution was added

to the respective wells in the fresh 96-well plate. Then absorbance of wells was measured using an ELISA plate reader (BioTek Instruments, Inc.) at 712 nm, 710 nm, and 687 nm (absorbance peak of fluorescent probes **A**, **B**, and **C**, respectively). Values of respective blanks were subtracted from samples (A_{dye}) and controls (A_{ctrl}). Cellular uptake efficiency was calculated as [1- (A_{dye} / A_{ctrl})]×100%.

2.6 MTS assay

MTS assay was performed with MDA-MB-231 cells (ATCC) as previously described.[36] Briefly, the cells were plated at a density of 5000 cells/well on a 96-well cell culture plate and incubated at 37 °C in 5% CO_2 incubator overnight. After incubation, the media was removed and the cells were washed with 1 X PBS. Fresh media with 0 μM, 5 μM, 15 μM, 25 μM, and 50 μM of fluorescent probes **A**, **B**, and **C** dissolved in DMSO (with less than <0.5% DMSO final concentration in media) were added to the wells and measured in 6 replicates for each dye concentration, respectively. Blanks that had everything else except the cells were prepared at the same time. The plates were incubated at 37 °C in 5% CO_2 incubator for 72 h. After the 72-hour incubation, 20 μL of MTS solution (from CellTiter 96 Aqueous Non-Radioactive Cell proliferation Assay (MTS) kit, Promega) was added to each well. The absorbance at 490 nm was acquired after 4-hour incubation at 37 °C, using an ELISA plate reader (BioTek Instruments, Inc.) Plots were normalized to control wells containing media and cells only.

3. Results and Discussion

3.1 Synthesis approach

In order to conjugate piperazine moiety into BODIPY dyes as parts of the fluorophores to modulate intramolecular charge transfer from the piperazine moieties to BODIPY cores (Scheme 2), we prepared 4-(4-methylpiperazin-1-yl)benzaldehyde (**3**) and 4-(4-(2-(2-(2-methoxyethoxy)ethoxy)ethyl)piperazin-1-yl)benzaldehyde (**5**) by reacting 4-fluorobenzaldehyde (**1**) with 1-methylpiperazine (**2**) and 1-(2-(2-(2-methoxyethoxy)ethoxy)ethyl)piperazine (**4**) in DMF solution under a basic condition at 80 °C, respectively. BODIPY-based near-infrared fluorescent probe **A** was prepared by incorporating piperazine residues into BODIPY cores at 3,5-positions via the Knoevenagel condensation reaction of our previously reported BODIPY dye (**7**) with 4-(4-methylpiperazin-1-yl)benzaldehyde (**3**). Fluorescent probe **A** is hydrophobic and displays very low solubility with less than 0.1 mg/mL in water. In order to enhance hydrophilic feature of the fluorescent probes, we prepared near-infrared emissive probes (**B** and **C**) by using hydrophilic 4-(4-(2-(2-(2-methoxyethoxy)ethoxy)ethyl)piperazin-1-yl)benzaldehyde (**5**) to conduct the Knoevenagel condensation reactions with BODIPY dye (**7**) and our previously reported water soluble BODIPY dye (**9**)**,** respectively. Probe **B** is more soluble (~1.0 mg/mL) than probe **A** in water while probe **C** shows excellent solubility with at least 20 mg/mL in aqueous solution. The hydrophilicity of fluorescent probes **B** and **C** are significantly enhanced because of the numerous hydrophilic oligo(ethylene glycol)methyl ether residues at meso- and 3,5-positions which significantly facilitate the strong enthalpic interactions with water molecules.

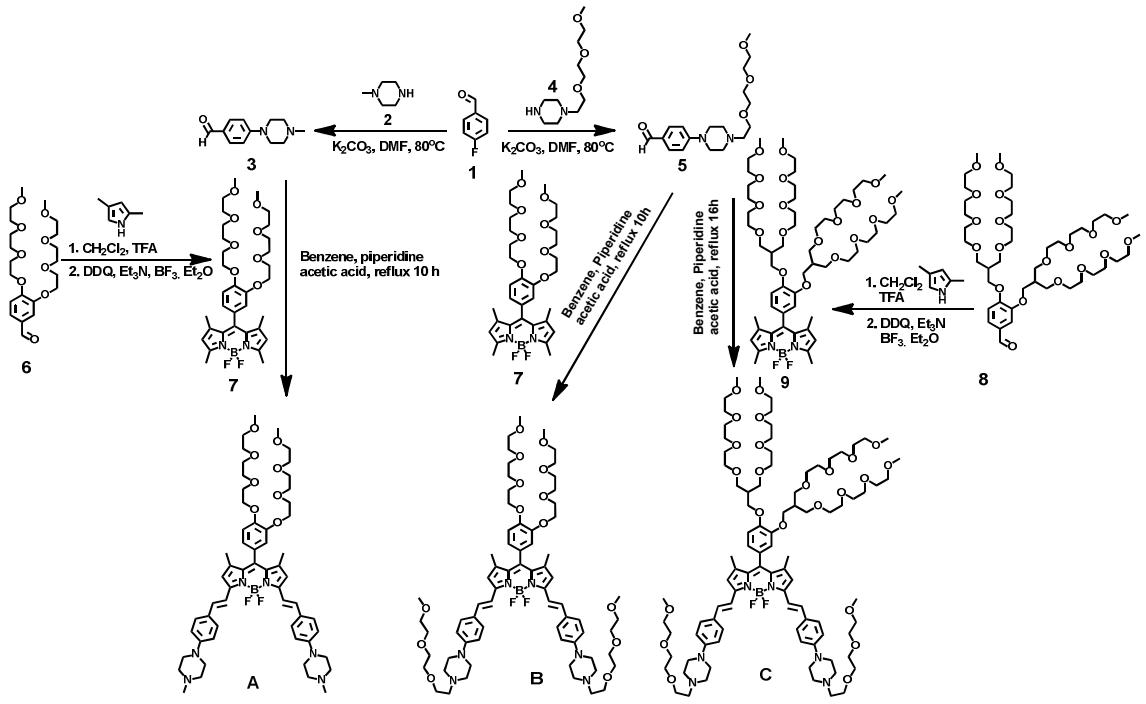

Scheme 2 Synthetic route to near-infrared fluorescent probes **A**, **B** and **C**.

Journal Name

RSCPublishing

ARTICLE

3.2 Optical properties of fluorescent probes

The absorption properties of BODIPY dye (**7**) in ethanol is characterized by a strong $S_0 \rightarrow S_1$ (π-π^*) transition at 499 nm and a weaker broad band around 350 nm attributed to the $S_0 \rightarrow S_2$ (π-π^*) transition. It shows fluorescent peak at 509 nm in ethanol solution. Fluorescent probe **A** displays significant red shifts in absorption and emission spectra in ethanol solution with absorption and emission peaks at 668 nm and 715 nm, respectively because of significantly enhanced π-conjugation and intramolecular charge transfer effect from piperazine moieties at 3,5-positions to the BODIPY core compared with BODIPY dye (**7**). The similar spectroscopic properties of probe **A** were obtained in dichloromethane and DMSO solutions. However, in aqueous solution the intramolecular charge transfer effect of the probe **A** becomes more significant because of polar solvent effect and potential dye aggregation may occur, which results in very low fluorescence and further red shifts in absorption and emission spectra of probe **A** with absorption and emission peaks at 712 nm and 770 nm in buffer (pH 7.4), respectively (Table 1). Fluorescent probe **B** exhibits similar optical properties to those of the probe **A** in organic solvents. But the absorption peak (710 nm) and emission peak (755 nm) of probe **B** in buffer solution (pH 7.4) were found slightly blue shifted compared with probe **A** (Table 1). This may be attributed to the reduced aggregation in aqueous solution with hydrophilic oligo(ethylene glycol)methyl ether residues on piperazine moieties at 3,5-positions. Highly water-soluble BODIPY dye (**9**) displays absorption and emission peaks at 500 nm and 509 nm in aqueous solution. Fluorescent probe **C** shows considerable red shifts in absorption and emission spectra with absorption peaks at 669 nm and 687 nm, and emission peaks at 720 nm and 750 nm in ethanol and buffer solution (pH 7.4), respectively (Table 1) because of its significant extended π-conjugation and intramolecular charge transfer effect from piperazine moieties at 3,5-positions to the BODIPY core compared with those of its precursor BODIPY dye **9**. Compared with the properties of probes **A** and **B**, the highly water-soluble character of probe **C** may further reduce its self-aggregation effect in buffer solution as it shows the shortest absorption and emission wavelength among three probes in buffer solution (pH 7.4). Light scattering measurements confirmed the presence of aggregated species of probes **A**, **B** and **C** in aqueous solution at pH 7.4 with average aggregation sizes (hydrodynamic diameter) of 500 nm, 334 nm and 272 nm, respectively. Decrease of pH to 4.5 reduces the aggregation sizes of fluorescent probes **A**, **B** and **C** to 391 nm, 174 nm and 82 nm respectively because of charge repulsion between BODIY dyes through protonation of piperazine moieties at lower pH. Further decrease of pH to 2.6 significantly reduces the aggregation size of probe **A** to 22 nm while probes **B** and **C** show no detectable aggregations in this condition. (Fig. S37-S40 in ESI†).

Table 1 Photophysical properties of probes **A**, **B** and **C** (protonation and non-protonation form). The protonation source in organic solvent is trifluoroacetic acid.

	solvent	λ_{abs} (nm)	λ_{em} (nm)	ε_{max} (10^4 $M^{-1}cm^{-1}$)	Φ_f (%)
7	Ethanol	499	509	9.10	72.1
9	Ethanol	500	509	7.14	61.0
A	CH_2Cl_2	675	722	7.10	4.3
	Ethanol	668	715	6.88	3.8
	DMSO	674	721	7.05	3.4
	Buffer (pH 7.4)	712	770	4.36	<0.01
A+H^+	CH_2Cl_2	658	690	7.58	11.5
	Ethanol	652	685	7.86	10.3
	Buffer (pH 2.6)	675	715	4.35	0.033
	Buffer (pH 4.5)	680	716	3.94	0.01
B	CH_2Cl_2	679	729	9.31	3.4
	Ethanol	670	720	8.56	2.8
	DMSO	676	724	9.27	3.0
	Buffer (pH 7.4)	710	755	5.20	<0.01
B+H^+	CH_2Cl_2	662	696	10.4	9.2
	Ethanol	653	683	11.2	10.3
	Buffer (pH 2.6)	669	715	5.60	0.06
	Buffer (pH 4.5)	675	715	4.60	0.02
C	CH_2Cl_2	675	722	7.76	4.5
	Ethanol	669	720	7.88	2.8
	DMSO	675	724	8.11	3.3
	Buffer (pH 7.4)	687	750	4.80	<0.01
C+H^+	CH_2Cl_2	661	694	8.55	9.9
	Ethanol	653	687	9.22	11.0
	Buffer (pH 2.6)	665	715	5.92	0.16
	Buffer (pH 4.5)	671	716	4.46	0.07

3.3 Optical responses of fluorescent probes to pH

We investigated pH effect on optical properties of fluorescent probes and their BODIPY precursors (**7**, **9**) in buffer solutions. We did this to verify our hypothesis that incorporation of piperazine moieties into BODIPY dyes at 3,5-positions can effectively modulate sensitive optical responses of BODIPY dyes to pH. BODIPY dyes **7** and **9** display no responses to pH

in absorption and emission in buffer solution, which are typical optical properties of typical BODIPY dyes (Fig. S20-S22 in electronic supplemental information ESI†). However, fluorescent probes **A**, **B** and **C** display very sensitive responses to pH in both absorption and emission (Fig. 1). Decreases of pH values from 9.98 to 2.20 cause significant increases in fluorescent intensities at 715 nm of fluorescent probes **A**, **B** and **C** with 75-, 88- and 102-fold enhancements, respectively (Fig. 1). In addition, there are significant blue shifts of 55 nm, 41 nm and 35 nm in emission spectra of the probes **A**, **B** and **C**, respectively, because of significantly reduced intramolecular charge transfer (ICT) effect from piperazine moieties to BODIPY cores through protonation of nitrogen atoms in piperazine moieties as well as reduced aggregation effect (Fig. S37-S40 in ESI†) in acidic conditions (Scheme 1), which is further confirmed by significant blue shifts of 46 nm, 53 nm and 23 nm in absorption spectra of fluorescent probes **A**, **B** and **C** when pH values of the buffer were changed from 9.98 to 2.20. Except ICT effect, fluorescence quenching caused by potential photo-induced electron transfer (PET) from lower nitrogen atoms of piperazine moieties at 3,5-positions of BODIPY core may also contribute to the extreme low fluorescence of all three probes in neutral condition. This fluorescence quenching effect could be reduced at low pH because the protonation of piperazine moieties can prohibit the PET process.

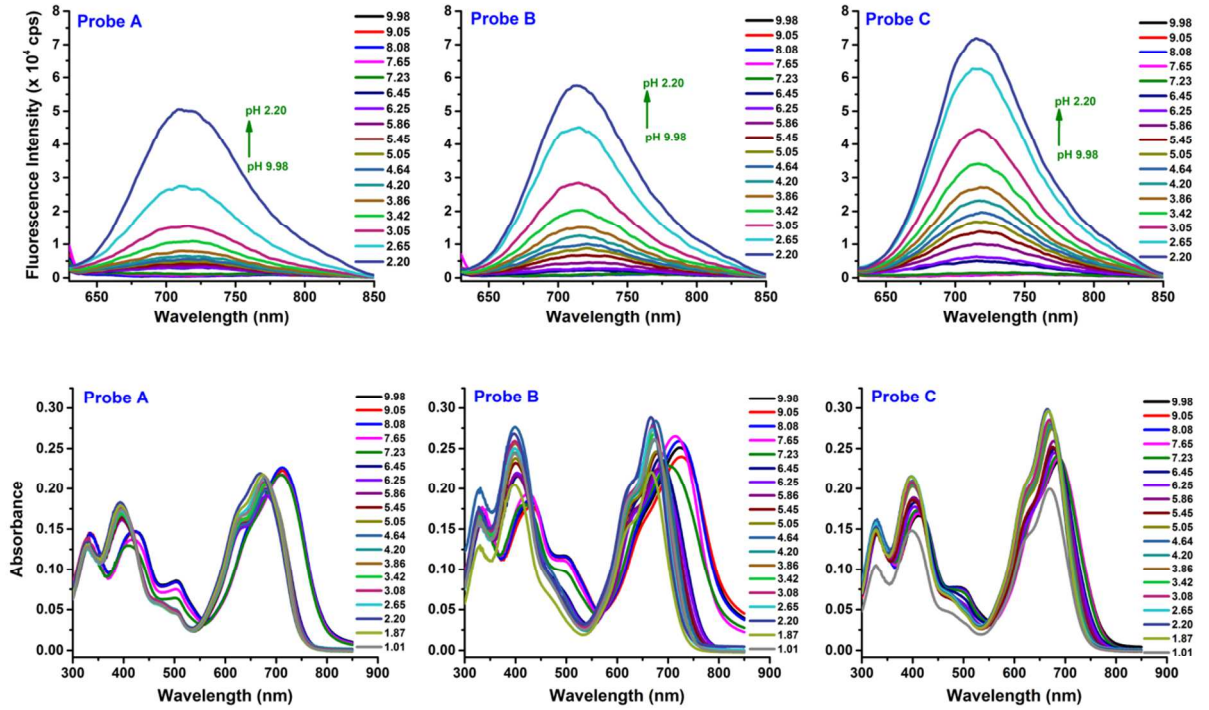

Fig. 1 Emission (upper row) and absorption (lower row) spectra of fluorescent probes **A**, **B** and **C** (5 μM) in buffer solution at different pH values.

Fig. 2 shows more detailed fluorescent intensity change at 715 nm of probes **A**, **B** and **C** at different pH conditions in buffer solution. From basic to neutral condition, all probes show very weak fluorescence without any obvious change. Their fluorescence intensities gradually increase when pH decreases from 7.0 to 2.2. The pK_a values of probes **A**, **B** and **C** are 2.91, 3.19 and 3.57 respectively (see supplementary information ESI† for method of pK_a calculations). Obviously, probe **C** exhibits highest fluorescence responses with highest pK_a value among all three probes. This indicates that the highly water-soluble probe **C** has less aggregation and it is protonated much more easily in aqueous solution. As a result, probe **C** displays more sensitivity to pH than probes **A** and **B**. In the pH window between physiological pH at 7.4 and lysosomal pH at 4.2, very good linear fluorescence responses were found for all probes in which probe **C** gives the highest sensitivity (Fig. 2 inset). From pH 7.4 to pH 4.2, the fluorescence intensities increased by 7-, 17- and 22-folds for probes **A**, **B** and **C**, respectively, and their fluorescence quantum yields at pH 4.5 also significantly increase compared with those in neutral pH condition at 7.4 (Table 1). These linear, high dynamic range and sensitive responses to pH indicate the feasibility of intracellular pH (pH_i) detection by using these probes. Further decreases of pH values from 2.20 to 1.5 results in significant fluorescence quenching of the probes (Fig. 2). We have eliminated the possibility of decomposition of the probes as the probes display stable reversible responses to pH between 1.5

and 10. However, the fluorescence quenching mechanism of the probes at extremely low pH needs further investigation.

In addition, we investigated the optical properties of the probes after protonation in organic solvents. After adding two equivalents of trifluoroacetic acid, the absorption and emission spectra of probe **A** immediately changed in ethanol and dichloromethane solution. The dramatic blue shifts both on absorption and emission were present with new absorption and emission peaks at 652 nm and 685 nm in ethanol, and 658 nm and 690 nm in dichloromethane solution, respectively. The fluorescence quantum yield of probe **A** is also enhanced by 2.71-fold in ethanol and 2.67-fold in dichloromethane solution. The disappearance of original peaks and presence of new blue shifted peaks indicate that probe **A** was fully protonated and the intramolecular charge transfer from nitrogen atoms at 3,5-positions to BODIPY core was prohibited which enhanced the fluorescence. Probes **B** and **C** exhibit the similar change after protonation in ethanol and dichloromethane. Surprisingly, there is no change after adding trifluoroacetic acid in DMSO solution of probes. It may be due to the relative high pK_a value of trifluoroacetic acid in DMSO (pK_a = 3.45).[37]

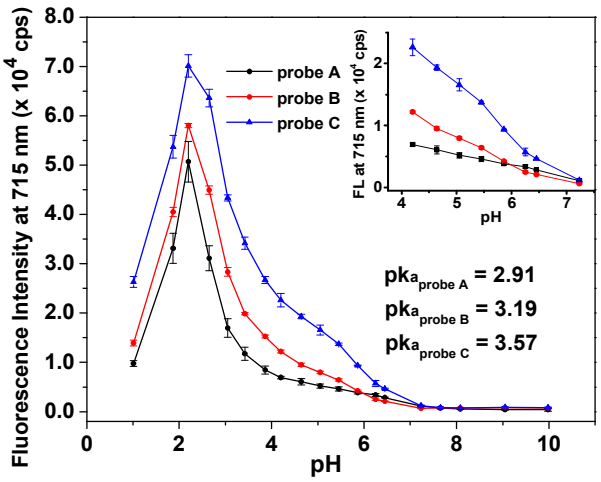

Fig. 2 Fluorescent responses of probes **A**, **B** and **C** to different pH values in buffer solution. Inset: zoomed fluorescence intensity responses of probes **A**, **B** and **C** to pH in the window between cytoplasm pH to lysosomal pH.

3.4 NMR study

In order to further study intramolecular charge transfer effect of piperazine moieties to BODIPY cores, we chose probe **B** and use ^{1}H NMR to investigate the structure change before and after protonation of the probe. Deuterium methanol (CD_3OD) was used as solvent for ^{1}H NMR measurement because it gave spectra with less peak overlaps than the spectra obtained in $CDCl_3$ solution. Fig. 3 shows the comparison of ^{1}H NMR spectra of probe **B** before and after its protonation in CD_3OD solution. Broad peaks were observed on the spectra of probe **B** due to the fast relaxation from its high polarity character and potential hydrogen bonding on the nitrogen atom of piperazine moiety. After adding two equivalents of trifluoroacetic acid, the spectra of the probe immediately changed. All peaks turned to be very sharp shape and protons **j** and **k** significantly shifted to down-filed (from 2.53 to 3.38 ppm) which indicates the protonation of the lower nitrogen atoms on piperazine moieties at 3,5-positions as it has more lone-pair availability to be protonated than the upper nitrogen atoms which were conjugated to BODIPY core. The neighbouring proton **i** also down-field shifted after protonation but with smaller change of 0.35 ppm (3.14 to 3.49 ppm). In addition, the aromatic protons **f** and **b** also underwent down-field shifts after protonation and these protons did not further shift with addition of more than two equivalents of the acid. These results further confirm our previous hypothesis that the proton is transferred or delocalized between the two nitrogen atoms of the piperazine moiety after protonation of the probes, which significantly reduces the electron donation ability of conjugated nitrogen atoms to the BODIPY core. Due to the protonation of the lower nitrogen atoms at 3,5-positions, photo-induced electron transfer from lower nitrogen atoms to BODIPY core may be prohibited which can also result in the great increase of fluorescent intensity at lower pH (Fig. 1).[38]

3.5 Solvent effect

Considering the nature of the intramolecular charge transfer (ICT) and potential self-aggregations on BODIPY dyes, we investigated the solvent polarity dependency of fluorescent probes **A**, **B** and **C** (Fig. 4). Optical properties of probes are highly dependent on solvent polarity and they exhibit the same changing patterns in their absorption and emission spectra in different polarity environments. Decreases of the solvent polarity by raising the percentage of ethanol in buffer solutions result in slight blue shifts of the fluorescent peaks, and significant fluorescence intensity enhancements of the probes. These changes may result from the reduced self-aggregation effect via fluorescence self-quenching, and more importantly from reduced intramolecular charge transfer (ICT) excited states of the fluorophores by nonpolar character of alcohol compared with water which recovers fluorescence given by more dominant locally excited (LE) states of the probes. Similar blue shifts in absorption spectra of the probes **A**, **B** and **C** were observed with increasing percentage of alcohol in the mixed buffer. However, the probes **A** and **B** show more blue shifts (44 nm and 40 nm) in their absorption peaks in pure ethanol solution than probe **C** which only gives an 18-nm shift. The more blue shifts in their absorption spectra in pure ethanol solution indicate that the probes **A** and **B** undergo potential aggregation in aqueous solution while the probe **C** has much weaker aggregation effect because of its highly water-soluble character as the bulky and hydrophilic branched oligo(ethylene glycol)methyl ether residues on the fluorophore could effectively prevent aggregation between BODIPY cores in aqueous solution.

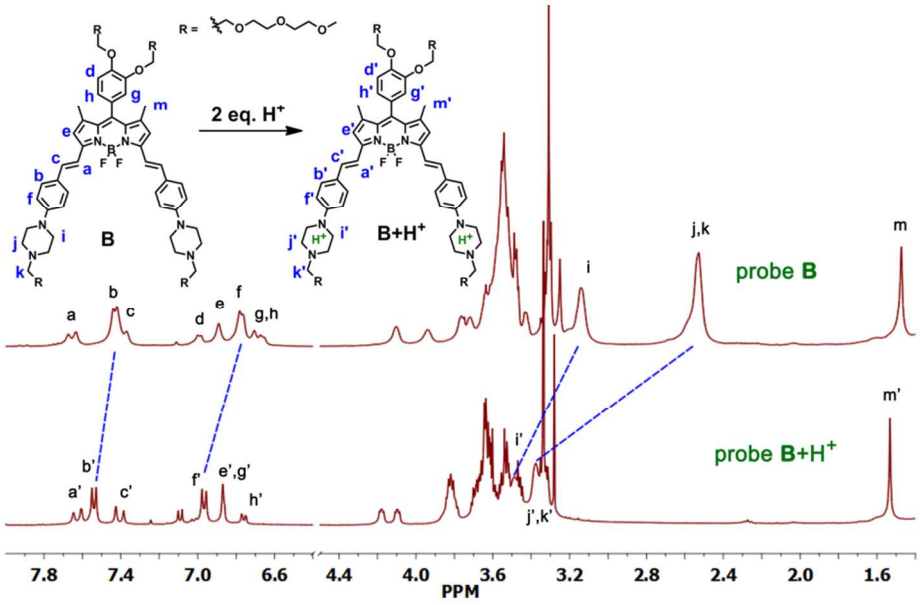

Fig. 3 ^{1}H NMR spectra (partial, peak **a** – **m**) of probe **B** before and after addition of two equivalents of trifluoroacetic acid in CD_3OD solution.

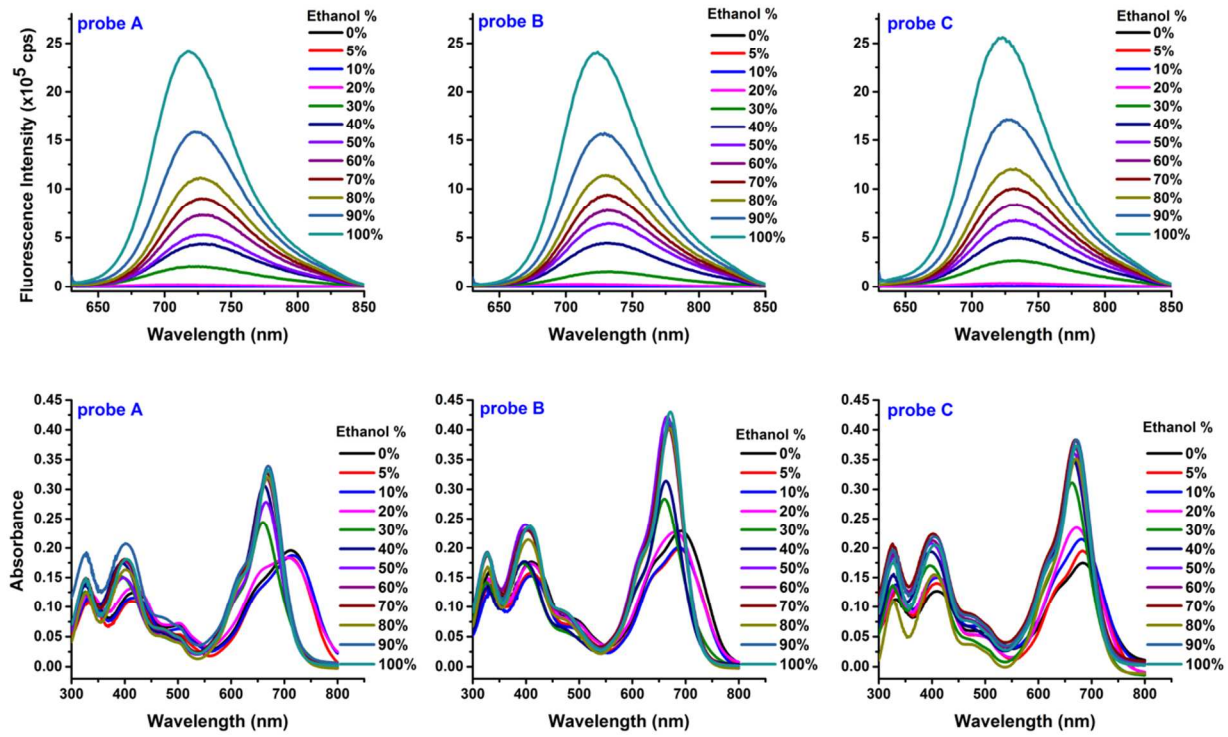

Fig. 4 Emission (upper row) and absorption (lower row) spectra of fluorescent probes **A**, **B** and **C** (5 μM) in mixed solvent (ethanol/buffer pH 7.4) with different percentages of ethanol.

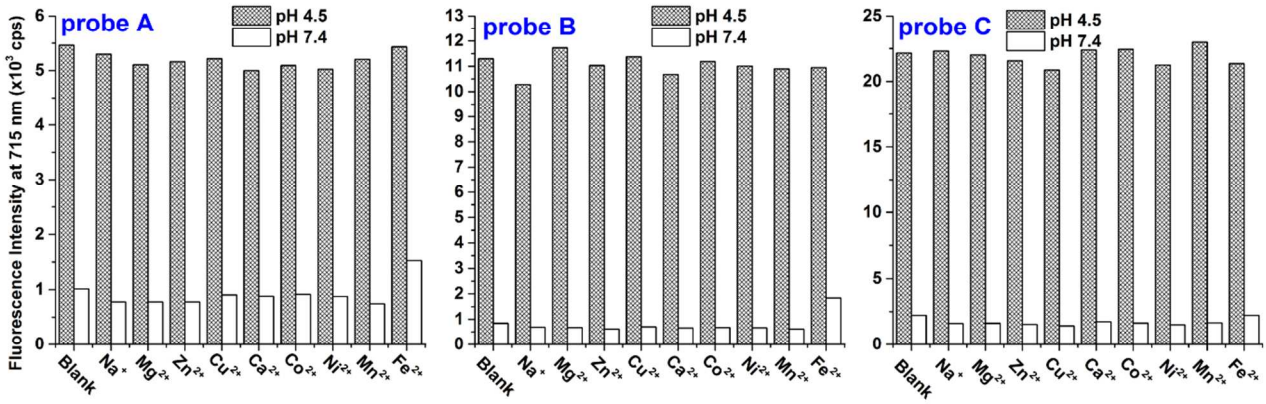

Fig. 5 Fluorescence responses of fluorescent probes **A**, **B** and **C** (5 μM) to different cations in pH 4.5 and 7.4 buffer solution.

3.6 Selectivity

We studied effect of different metal ions on fluorescent responses of fluorescent probes to pH and investigated potential coordination of fluorescent probes with heavy, transition, and main group metal ions. The fluorescent probes display high selectivity to pH over these alkali, alkaline-earth metal ions, and transitional metal ions because fluorescent probes **A**, **B** and **C** display no responses to 200 μM alkali and alkaline-earth metal ions as such Na^+, Mg^{2+} and Ca^{2+}, as well as some transitional metal ions (200 μM) such as Zn^{2+}, Cu^{2+}, Co^{2+}, Ni^{2+}, Mn^{2+} and Fe^{2+}, at both pH 7.4 and 4.5 (Fig. 5).

In addition, we investigated the potential effect of biological thiol such as cysteine on our probes. The results showed that there are negligible changes of the absorption and fluorescence spectra of 5 μM probes **A**, **B** and **C** in buffer solution after addition of 20 μM cysteine to the buffer solution at pH 7.4 and 4.5 within 30 minutes (Fig. S24–S25 in ESI†). This indicates that our probes are stable in presence of cysteine and the responses of the probes to pH are not interfered by cysteine.

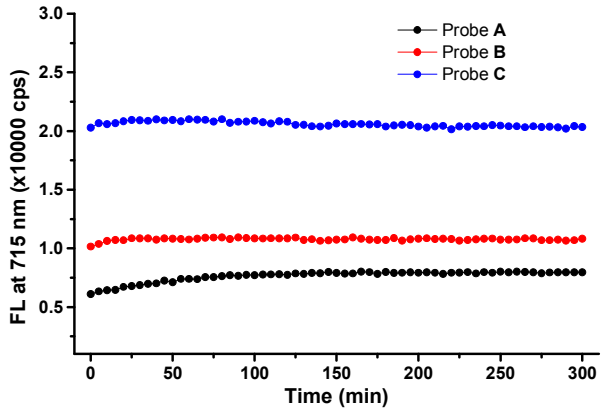

Fig. 6 Fluorescence intensities at 715 nm of probes **A**, **B** and **C** (5 μM) as function of time in 5 hours under excitation (620 nm) in citrate-phosphate buffer (pH 4.5).

3.7 Photostability

The photostability measurement was carried in buffer solution at pH 4.5. Fluorescent probes were excited continuously at 620 nm for 5 hours and fluorescence intensity was measured every 5 minutes. The result clearly showed that there was no significant decrease of the fluorescence intensity under 5-hour excitation for all three probes (Fig. 6). The fluorescence intensities of probes **A** and **B** increased by 20% and 7% in first 80 and 30 minutes respectively, and keep almost constant level after that. These increases may arise from the slow protonation of probes **A** and **B** because of their relative low solubility in aqueous solution. Probe **C** exhibited very stable fluorescent emission in first 2 hours under excitation and only 2% of fluorescence intensity decreased after 5-hour excitation.

3.8 Fluorescence responses in living cells

To find out if probes **A**, **B**, and **C** could selectively stain lysosomes or acidic organelles in cells, all three probes were compared with commercial probe LysoSensor Green DND-189, a known lysosome probe that specifically fluorescently stains acidic organelles in cells. Live cell imaging in various concentrations of probes **A**, **B**, and **C** were conducted using two cell lines: breast cancer cell line MDA-MB-231 and normal endothelial cell line HUVEC-C (Fig. 7 and 8). In both cell types, probes **A** and **B** showed very strong fluorescence signals and probe **C** showed weak fluorescence signal inside cells. The area in the cell stained with probe **A**, **B** or **C** matched those stained with LysoSensor Green DND-189. This suggests that these new probes are able to target lysosomes or other acidic cellular compartments in cells in a manner similar to LysoSensor Green DND-189 and distinguish between different regions inside cells based on pH. Co-localization analysis based on the Pearson's coefficient showed value of 0.85 or higher for probes **A**, **B**, and **C** with LysoSensor Green DND-189 indicating presence of both probes in the same cellular compartment (Fig. S34 in ESI†). The enlarged 60x magnification images from both cell lines (Fig. S32-33 in ESI†)

show high fluorescent area localized in the perinuclear region, which is in line with a previous report that shows lysosomes localized in the perinuclear region in clusters after serum starvation.[39, 40] Probe **A** showed the highest fluorescent intensity among all three probes and displayed good signal even at 2 μM concentration (Fig. S26, S29 in ESI†). The fluorescent signals from probe **B** was not as strong as probe **A**, but it showed measurable signal at 5 μM concentration and at higher concentrations (Fig. S27, S30 in ESI†). However, probe **C**, the most hydrophilic compound among the three probes, showed poor fluorescent signal even at high concentration of 25 μM (Fig. S28, S31 in ESI†). One of the possible reasons for this difference could be that probes **A** and **B** are more hydrophobic and less steric hindered than probe **C**, so they could easier bind or interact with lipophilic structures like micelles, lipososomes, membranes in lysosomes which further activate the fluorescence by depressing ICT effect of the fluorophores.[41]

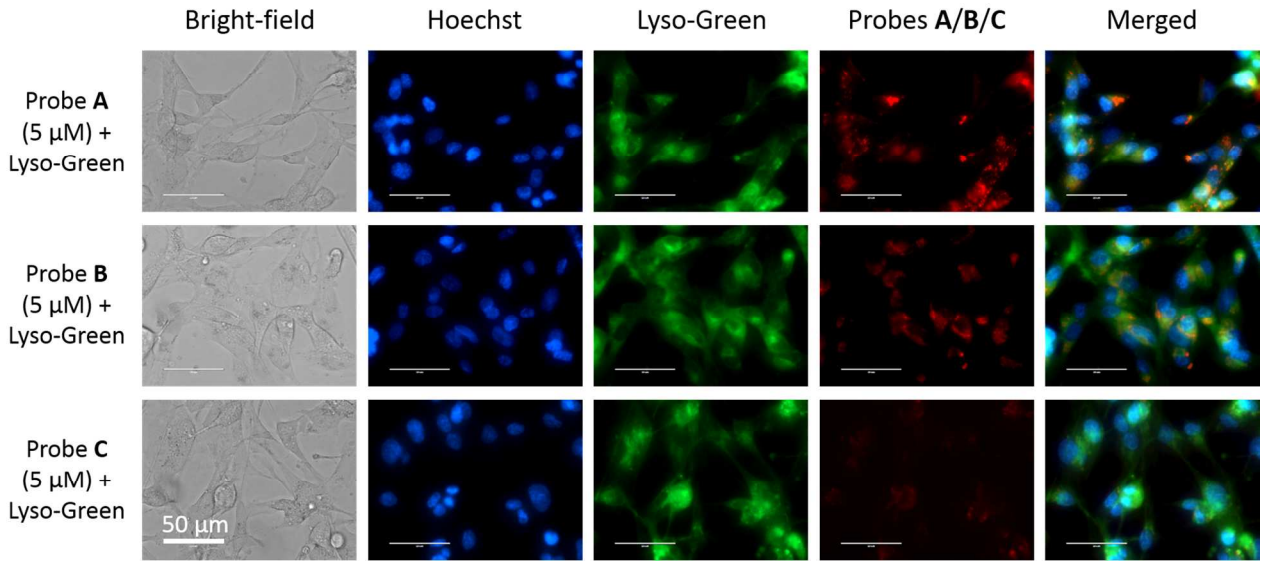

Fig. 7 Fluorescence images of MDA-MB-231 cells incubated with fluorescent probes **A**, **B**, and **C**. Cells incubated with 5 μM of respective probes for 2 h, post serum starvation (2 h) and imaged for co-localization with 1 μM LysoSensor Green and (1 μg/mL) Hoechst 33342 stains. All images were acquired at 60x magnification using inverted fluorescence microscope (AMF-4306, $EVOS_{fl}$, AMG).

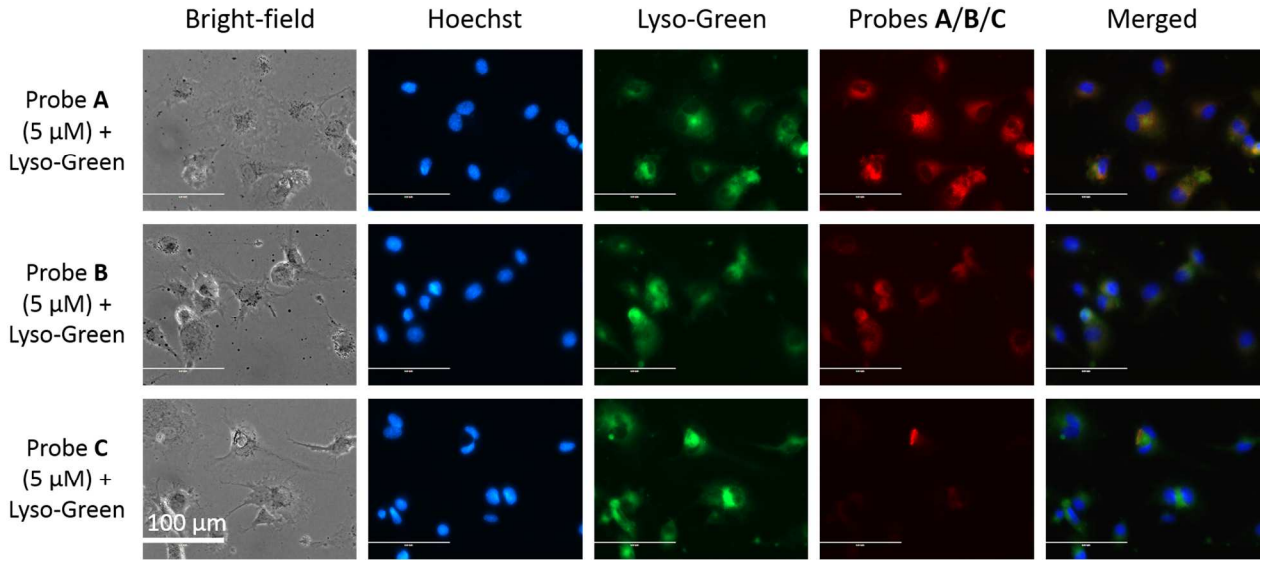

Fig. 8 Fluorescence images of HUVEC-C cells incubated with fluorescent probes **A**, **B**, and **C**. HUVEC-C cells were incubated with 5 μM of respective probes for 2 h, post serum starvation (2 h) and imaged for co-localization with 1 μM LysoSensor Green and (1 μg/mL) Hoechst 33342 stains. Images were acquired using the using inverted fluorescence microscope (AMF-4306, $EVOS_{fl}$, AMG) at 40X magnification.

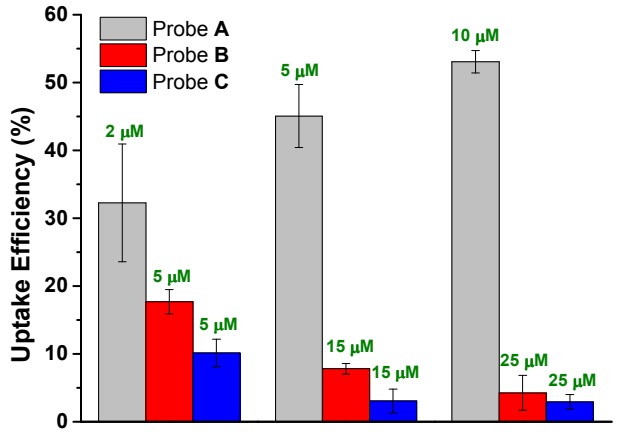

Fig. 9 The HUVEC-C cells cellular uptake efficiency of probes **A**, **B** and **C** at different concentrations after two hour incubations. The cellular uptake efficiency was calculated as the percentage of probe taken up by cells out of total amount of probe in initial incubation solution. Cell density = 1×10^4 cells/well.

It should be noted that the intensity of fluorescence in living cells is also dependent on the cellular uptake. Therefore, we further investigated the cellular uptake of HUVEC-C cells with different incubation concentrations of probes **A**, **B** and **C** (Fig. 9). The cellular uptake efficiency was calculated as the percentage of probe taken up by cells out of total amount of probe in initial incubation solution. The results showed probe **A** has much higher cellular uptake (more than 30%) at all three incubation concentrations compared with probes **B** and **C**. Probe **B** has moderate cellular uptake efficiency of 18% at incubation concentration of 5 μM but higher concentrations of 15 μM and 25 μM only give 8% and 4% uptake efficiency, respectively. Probe **C** showed the lowest cellular uptake efficiency with 10%, 3% and 3% for incubation concentration of 5 μM, 15 μM and 25 μM, respectively. This low cellular uptake of probe **C** could be the main reason for its relatively weak signals of the fluorescence images in living cells compared with probes **A** and **B**.

In order to examine the pH dependency of the probes inside the living cells, we conducted live cell fluorescence imaging at different intracellular pH values. In this study, HUVEC-C cells were incubated with 5 μM probe **A**, 15 μM probe **B** or 15 μM probe **C**, respectively, and then with nigericin (5 μg mL^{-1}) in buffer solution at different pH values from 5.0, 5.5, 6.0 to 7.5 to equilibrate the intracellular and extracellular pH. This is a standard approach that has been widely used to calibrate the intracellular pH (pH_i).[41-45] The probe **C** displayed very weak fluorescence in cells near physiological pH (pH 7.5) while its fluorescence intensity was significantly enhanced as pH decreased from 7.5 to 5.0 (Fig. 10). This turn-on response of probe **C** to acidic pH_i is in line with the trend of its pH response in buffer solution, which indicates that probe **C** is sensitive to pH not only in buffer solution, but also inside the living cells because of reduced ICT effect and potential photo-induced electron transfer effect from piperazine moieties to BODIPY core through protonation. Compared with probe **C**, commercial probe LysoSensor Green did not display any obvious change of fluorescence at different pH_i values. Probes **A** and **B** exhibited similar response to different pH_i as probe **C**, but with smaller fluorescence enhancements when pH_i decreased from 7.5 to 5.0 (Fig. S35-S36). This difference may be due to the fact that probe **C** has higher pK_a value and better water solubility than probes **A** and **B**.

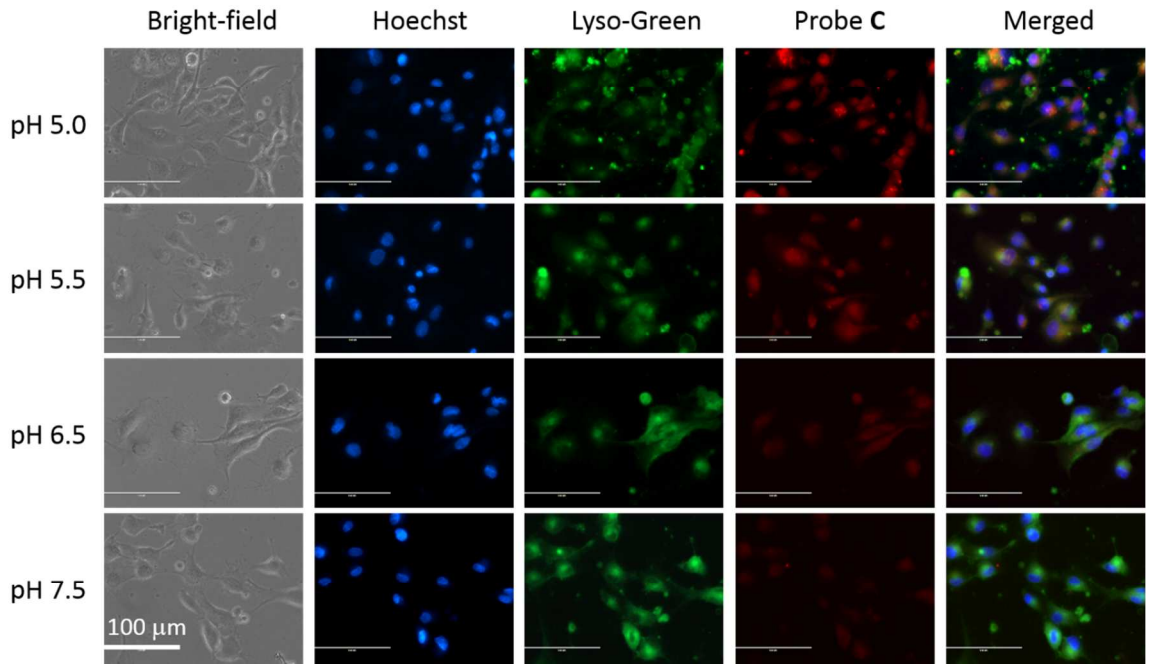

Fig. 10 Fluorescence images of HUVEC-C cells incubated with 15 μM probes **C** at different pH values. 1 μM LysoSensor Green and 1 μg/mL Hoechst 33342 were used as co-stains. Images were acquired using the using inverted fluorescence microscope (AMF-4306, EVOS$_{fl}$, AMG) at 40X magnification.

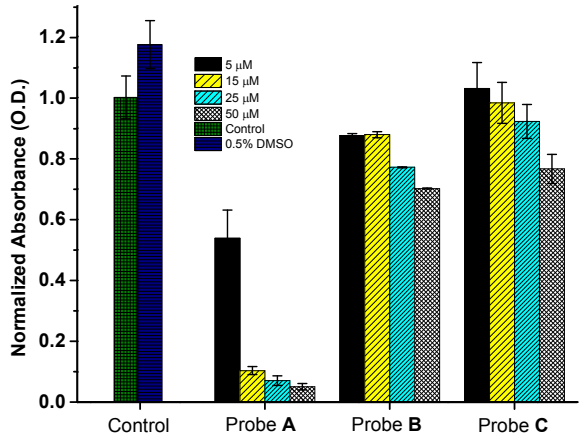

Fig. 11 Cytotoxicity and cell proliferation effect of probes **A**, **B** and **C** tested by MTS assay. The MDA-MB-231 cells were incubated with 5, 15, 25, and 50 μM of probes **A**, **B** and **C** for 72 h and cell viability was measured by adding MTS reagent and measuring the formation of formazon at 490 nm. Cell viability is directly proportional to the absorbance measured at 490 nm and was normalized to control cells (no probe added). The error bars indicate ± S.D. from 6 replicates.

MTS assay were performed to investigate the toxicity of these probes to cells (Fig. 11). Incubating the cells with the probes for 72 h shows that probe **A** has the highest cytotoxicity among the three probes with ~50% viability observed for cells incubated with 5 μM that dropped down to less than 10% viability at 15 μM and higher probe concentration (Fig. 11). In comparison, probes **B** and **C** showed very mild toxicity with greater than 70% cell viability even at 50 μM concentration (Fig. 11).

4. Conclusion

We have prepared three BODIPY-based near-infrared fluorescent probes **A**, **B** and **C** for lysosomal pH. The response mechanism of the fluorescent probes to pH value relies on modulation of intramolecular charge transfer and potential photo-induced electron transfer of piperazine moieties at 3,5-positions to BODIPY cores. These probes displays extremely low fluorescent at neutral pH because of intramolecular charge transfer and potential photo-induced electron transfer from piperazine moieties to BODIPY cores, and become highly fluorescent at low pH due to the significantly reduced intramolecular charge transfer effect and potential photo-induced electron transfer effect. These fluorescent probes are cell-permeable and provide selective and sensitive labelling of lysosomes for potential non-invasive monitoring of lysosomal pH changes during physiological and pathological processes.

Acknowledgments

This work was partially supported by National Science Foundation (to H.Y. Liu), and Michigan Technological University faculty start-up fund, and Research Excellence Fund (to A. Tiwari).

Notes and references

[a] Department of Chemistry, Michigan Technological University, Houghton, MI 49931
[b] Institute of Chemistry, Academia Sinica, Taipei, Taiwan 11529, Republic of China

† Electronic Supplementary Information (ESI) available: [The details of spectroscopic analysis, synthesis procedures of compound **3** and **5**, NMR spectra, absorption and emission spectra of probe **A**, **B** and **C** in different solvents, the spectroscopic responses of BODIPY dye **7** and **9** to different pH and fluorescence images of both cell lines with probe **A**, **B** and **C** at different concentrations are included.]. See DOI: 10.1039/b000000x/

1. A. C. Johansson, H. Appelqvist, C. Nilsson, K. Kagedal, K. Roberg and K. Ollinger, *Apoptosis*, 2010, **15**, 527-540.
2. B. Turk and V. Turk, *J. Biol. Chem.*, 2009, **284**, 21783-21787.
3. J. Stinchcombe, G. Bossi and G. M. Griffiths, *Science*, 2004, **305**, 55-59.
4. E. J. Blott and G. M. Griffiths, *Nat. Rev. Mol. Cell Biol.*, 2002, **3**, 122-131.
5. Z. J. Diwu, C. S. Chen, C. L. Zhang, D. H. Klaubert and R. P. Haugland, *Chem. Biol.*, 1999, **6**, 411-418.
6. H. S. Lv, J. Liu, J. Zhao, B. X. Zhao and J. Y. Miao, *Sens. Actuator B-Chem.*, 2013, **177**, 956-963.
7. H. Zhu, J. L. Fan, Q. L. Xu, H. L. Li, J. Y. Wang, P. Gao and X. J. Peng, *Chem. Commun.*, 2012, **48**, 11766-11768.
8. Z. Li, Y. L. Song, Y. H. Yang, L. Yang, X. H. Huang, J. H. Han and S. F. Han, *Chem. Sci.*, 2012, **3**, 2941-2948.
9. L. Q. Ying and B. P. Branchaud, *Bioorg. Med. Chem. Lett.*, 2011, **21**, 3546-3549.
10. D. G. Smith, B. K. McMahon, R. Pal and D. Parker, *Chem. Commun.*, 2012, **48**, 8520-8522.
11. L. J. Ma, W. G. Cao, J. L. Liu, D. Y. Deng, Y. Q. Wu, Y. H. Yan and L. T. Yang, *Sens. Actuator B-Chem.*, 2012, **169**, 243-247.
12. F. Galindo, M. I. Burguete, L. Vigara, S. V. Luis, N. Kabir, J. Gavrilovic and D. A. Russell, *Angew. Chem. Int. Ed.*, 2005, **44**, 6504-6508.
13. H. M. DePedro and P. Urayama, *Anal. Biochem.*, 2009, **384**, 359-361.
14. T. Hasegawa, Y. Kondo, Y. Koizumi, T. Sugiyama, A. Takeda, S. Ito and F. Hamada, *Biorg. Med. Chem.*, 2009, **17**, 6015-6019.
15. H. J. Lin, P. Herman, J. S. Kang and J. R. Lakowicz, *Anal. Biochem.*, 2001, **294**, 118-125.
16. J. Y. Han and K. Burgess, *Chem. Rev.*, 2010, **110**, 2709-2728.
17. J. L. Fan, H. J. Dong, M. M. Hu, J. Y. Wang, H. Zhang, H. Zhu, W. Sun and X. J. Peng, *Chem. Commun.*, 2014, **50**, 882-884.
18. J. L. Fan, C. Y. Lin, H. L. Li, P. Zhan, J. Y. Wang, S. Cui, M. M. Hu, G. H. Cheng and X. J. Peng, *Dyes Pigment.*, 2013, **99**, 620-626.

19. H. Zhang, J. L. Fan, H. J. Dong, S. Z. Zhang, W. Y. Xu, J. Y. Wang, P. Gao and X. J. Peng, *J. Mater. Chem. B*, 2013, **1**, 5450-5455.
20. X. F. zhang, C. Wang, Z. Han and Y. Xiao, *ACS Appl. Mater. Interfaces*, 2014, **6**, 21669–21676.
21. L. Wang, Y. Xiao, W. M. Tian and L. Z. Deng, *J. Am. Chem. Soc.*, 2013, **135**, 2903-2906.
22. G. P. Li, D. J. Zhu, L. Xue and H. Jiang, *Org. Lett.*, 2013, **15**, 5020-5023.
23. P. Li, H. Zhou and B. Tang, *J. Photochem. Photobio. a-Chem.*, 2012, **249**, 36-40.
24. X. B. Wang, X. Y. Ma, Z. Yang, Z. Zhang, J. H. Wen, Z. R. Geng and Z. L. Wang, *Chem. Commun.*, 2013, **49**, 11263-11265.
25. Z. G. Wu, M. L. Tang, T. Tian, J. G. Wu, Y. L. Deng, X. H. Dong, Z. Tan, X. C. Weng, Z. H. Liu, C. J. Wang and X. Zhou, *Talanta*, 2011, **87**, 216-221.
26. L. Xue, G. P. Li, D. J. Zhu, Q. Liu and H. Jiang, *Inorg. Chem.*, 2012, **51**, 10842-10849.
27. Z. Q. Hu, M. Li, M. D. Liu, W. M. Zhuang and G. K. Li, *Dyes Pigment.*, 2013, **96**, 71-75.
28. H. Lee, W. Akers, K. Bhushan, S. Bloch, G. Sudlow, R. Tang and S. Achilefu, *Bioconjug. Chem.*, 2011, **22**, 777-784.
29. C. Li, T. R. Greenwood and K. Glunde, *Neoplasia*, 2008, **10**, 389-398.
30. X. H. Wang, D. M. Nguyen, C. O. Yanez, L. Rodriguez, H. Y. Ahn, M. V. Bonder and K. D. Belfield, *J. Am. Chem. Soc.*, 2010, **132**, 12237-12239.
31. G. K. Vegesna, J. Janjanam, J. H. Bi, F.-T. Luo, J. T. Zhang, C. Olds, A. Tiwaria and H. Y. Liu, *J. Mater. Chem. B*, 2014, **2**, 4500-4508.
32. S. Zhu, J. Zhang, G. Vegesna, F.-T. Luo, S. A. Green and H. Liu, *Org. Lett.*, 2011, **13**, 438-441.
33. S. L. Zhu, J. T. Zhang, G. K. Vegesna, R. Pandey, F. T. Luo, S. A. Green and H. Y. Liu, *Chem. Commun.*, 2011, **47**, 3508-3510.
34. S. L. Zhu, J. T. Zhang, J. Janjanam, J. H. Bi, G. Vegesna, A. Tiwari, F. T. Luo, J. J. Wei and H. Y. Liu, *Anal. Chim. Acta*, 2013, **758**, 138-144.
35. S. Bolte and F. P. Cordelieres, *J. Microsc-Oxford,* 2006, **224**, 213-232.
36. X. C. Ding, J. Janjanam, A. Tiwari, M. Thompson and P. A. Heiden, *Macromol. Biosci.*, 2014, **14**, 853-871.
37. F. G. Bordwell, *Acc. Chem. Res.*, 1988, **21**, 456-463.
38. C. B. Huang, J. L. Qu, J. Qi, M. Yan and G. X. Xu, *Org. Lett.*, 2011, **13**, 1462-1465.
39. C. Pous and P. Codogno, *Nat. Cell Biol.*, 2011, **13**, 342-344.
40. G. K. Vegesna, J. Janjanam, J. H. Bi, F. T. Luo, J. T. Zhang, C. Olds, A. Tiwari and H. Y. Liu, *J. Mater. Chem. B*, 2014, **2**, 4500-4508.
41. J. A. Thomas, R. N. Buchsbaum, A. Zimniak and E. Racker, *Biochemistry (Mosc).* 1979, **18**, 2210-2218.
42. J. Llopis, J. M. McCaffery, A. Miyawaki, M. G. Farquhar and R. Y. Tsien, *Proc. Natl. Acad. Sci. U. S. A.*, 1998, **95**, 6803-6808.
43. L. Fan, Q. L. Liu, D. T. Lu, H. P. Shi, Y. F. Yang, Y. F. Li, C. Dong and S. M. Shuang, *J. Mater. Chem. B*, 2013, **1**, 4281-4288.
44. P. S. Song, X. T. Chen, Y. Xiang, L. Huang, Z. J. Zhou, R. R. Wei and A. J. Tong, *J. Mater. Chem.*, 2011, **21**, 13470-13475.
45. J. Y. Han, A. Loudet, R. Barhoumi, R. C. Burghardt and K. Burgess, *J. Am. Chem. Soc.*, 2009, **131**, 1642-+.

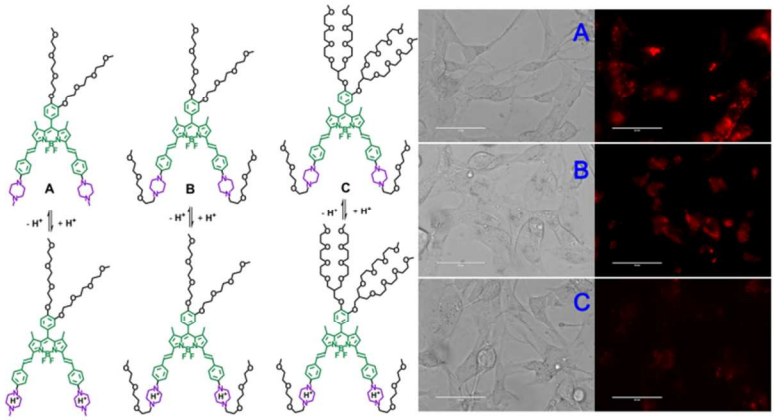

Three BODIPY-based near-infrared fluorescent probes have been synthesized, characterized, and evaluated for sensing and imaging of lysosomal pH inside living cells.